Photodriven Ammonia Synthesis from Manganese Nitrides: Photophysics and Mechanistic Investigations

Grace B. Panetti[†], Junho Kim[†], Michele S. Myong[‡], Matthew J. Bird[‡]*, Gregory D. Scholes,[†]* and Paul J. Chirik[†]*

†Department of Chemistry, Frick Laboratory, Princeton University, Princeton, New Jersey 08544, United States

‡Chemistry Division, Brookhaven National Laboratory, Upton, New York 11973, United States

KEYWORDS proton coupled electron transfer, ammonia, manganese, nitride, ultrafast spectroscopy, mechanism, acridine

ABSTRACT: Ammonia synthesis from N,N,O,O-supported manganese (V) nitrides and 9,10-dihydroacridine using proton-coupled electron transfer and visible light irradiation in the absence of a precious metal photocatalyst is described. While the reactivity of the nitride correlated with increased absorption of blue light, excited-state lifetimes determined by transient absorption were on the order of picoseconds. This eliminated excited state manganese nitrides as responsible for bimolecular N–H bond formation. Spectroscopic measurements on the hydrogen source, dihydroacridine, demonstrated that photooxidation of 9,10-dihydroacridine was necessary for productive ammonia synthesis. The transient absorption and pulse radiolysis data for dihydroacridine provided evidence for the presence of intermediates with weak E–H bonds, including the dihydroacridinium radical cation and both isomers of monohydroacridine radical. Additional optimization of the reaction conditions using catalytic amounts of acridine, resulted in higher rates of the ammonia production from the manganese(V) nitrides due to introduction of a photooxidant.

INTRODUCTION

Metal nitrides are of broad interest due to applications in materials science and coordination chemistry.[1] Notably, terminal transition metal nitrides serve as the nitrogen source in both atom transfer and ammonia synthesis chemistry.[2] However, the thermodynamic stability of most isolable metal nitrides results in *weak* N–H bonds in the corresponding imido complexes.[3] One approach to overcoming this energetic limitation is the use of separate proton and electron sources that by formation of stoichiometric byproducts incur large chemical overpotentials.[3c,4]

Alternatively, molecules containing weak element-hydrogen (E–H) bonds are attractive for forming N–H bonds from thermodynamically stable metal nitrides. Those with BDFEs less than 50 kcal mol^{-1} are of particular interest to promote additional chemistry.[5] Various alternative approaches have been explored to activate molecules to reduce BDFEs and enable productive H-atom transfer chemistry. Strategies include coordination to a metal (coordination-induced bond weakening), photon absorption, redox chemistry or H-atom transfer events (Scheme 1b).[5b,6] While irradiation with visible light has been posited, photoredox methods have dominated as an effective strategy for generating reactive intermediates with low effective BDFEs.[7] These approaches have been used extensively for the formation and cleavage of E–H bonds through proton-coupled electron transfer (PCET) with implications in biochemistry and organic chemistry and activation of metal-ligand multiple bonds.[5]

Scheme 1. Metal nitrides and the production of weak E–H bonds either by coordination, redox, light absorption or H-atom transfer events.

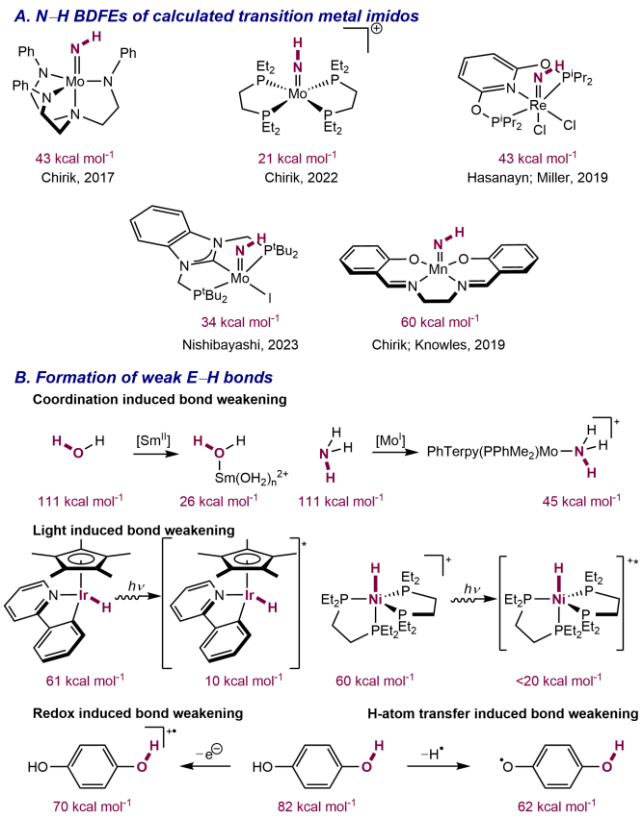

The application of photoinduced PCET to generate weak E–H bonds for subsequent N–H bond formation with metal nitrides has been demonstrated as a distinct route for ammonia synthesis (Scheme 2A).[3c] Blue light irradiation of salen-supported manganese nitrides in the presence of a ruthenium photocatalyst, acid and 9,10-dihydroacridine (H_2Acr) as the terminal reductant was effective for ammonia synthesis.[6g,8] Related work by Nishibayashi and coworkers demonstrated catalytic ammonia synthesis using a PCP pincer molybdenum complex, an iridium photocatalyst, and H_2Acr.[9] Peters and coworkers have also applied this approach to catalytic ammonia synthesis using a PNP pincer molybdenum complex, an iridium photocatalyst, and a Hantzsch ester as the stoichiometric H-atom source.[10] In all of the reported examples, ammonia formation was observed, albeit in significantly lower yields in the absence of the precious metal photocatalyst. These observations raise questions as to the nature of the photoactive compound in solution responsible for N–H bond formation. Despite extensive photophysical measurements on terminal metal oxides[11] and metal alkylidynes,[12] related studies on the photophysics of metal nitrides are comparatively rare and principally focused on luminescence.[13]

Scheme 2. Photocatalytic production of ammonia using metal nitrides

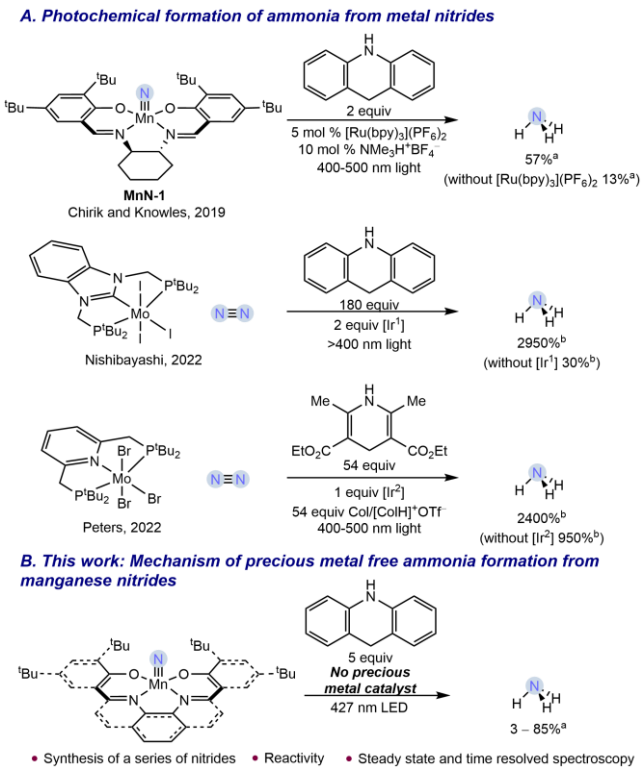

A. Previous examples of photo-induced formation of ammonia. Examples are shown with and without photocatalyst. [a]Yield of ammonia reported versus added Mn species. [b]Yield of ammonia reported versus added Mo species. [Ir[1]] = [iridium bis(2-(2-pyridyl)phenyl)(4,4′-di-tert-butyl-2,2′-bipyridine] [$SO_3C_4F_9$]; [Ir[2]] = [iridium bis(2-(4-trifluoromethyl 2-pyridyl) -3,5-difluoro-phenyl)(4,4′-di-tert-butyl-2,2′-bipyridine][tetrakis (3,5-trifluoromethyl phenyl) borate]. B. Mechanistic study and optimization of manganese-based precious metal free photo-ammonia production.

Here we describe the exploration of the origin and mechanism of light-driven ammonia formation from manganese nitrides in the absence of a precious metal photocatalyst (Scheme 2B). The synthesis and isolation of multiple manganese nitrides is reported and their ground state spectroscopy and electrochemical data are described. The BDFEs of previously proposed intermediates indicate that the formation of either the manganese (IV) imido or acridine radical are responsible for ammonia formation. Using transient absorption pump-probe spectroscopy, the lifetimes of salen-supported manganese nitrides were measured and determined to be significantly shorter than the required lifetime to engage in diffusion-based reaction chemistry. Instead, light absorption of acridine derivatives is responsible for the initiation of N–H bond formation and subsequent ammonia production.

RESULTS AND DISCUSSION

Synthesis and Spectroscopy of Manganese(V) Nitride Derivatives. One hypothesis for the photoproduction of ammonia in the absence of a precious metal photocatalyst relies on excitation of the manganese nitride by visible light to engage in subsequent N–H bond formation. Because only one example of a salen-supported manganese nitride (**MnN-1**) was examined for ammonia synthesis,[6g,8] ligand modifications were explored to systematically evaluate the role of blue light absorption. Related acacen **L-3** was targeted to absorb shorter wavelength light with a lower extinction coefficient, while both salophen **L-2** and bis-phenoxyphenanthrolene **L-4** were expected to absorb light of higher wavelength with a higher molar extinction coefficient. The corresponding manganese nitrides were synthesized either by initial treatment of the proligand with an excess of $Mn(OAc)_2$•4(H_2O) followed by a quench with a saturated NaCl solution or treatment of the proligand with 3 equivalents of NEt_3 and 3 equivalents of $MnCl_2(OH_2)_4$ to obtain the putative manganese(III) chloride. In all three cases, these intermediates were used without further purification. The resulting brown solids were then treated first with an excess of NH_4OH at 0 °C in a methylene chloride/methanol mixture followed by dropwise addition of a solution of 8% w/w $NaOCl_{(aq)}$. Each of the isolated manganese nitrides was characterized by X-ray diffraction and molecular geometries similar to **MnN-1** were observed in all cases.[14] The geometries of the pentacoordinate complexes are best described as idealized square pyramidal where the nitrogen atom occupies the apical position. The Mn–N distances in all four molecules range between 1.5192(6) and 1.530(4) Å and are statistically indistinguishable. Interrogation of the Mn–N stretching frequency by infrared spectroscopy produced values between 1049–1053 cm^{-1} and is consistent with a strong metal-nitrogen triple bond for each member of the series (Figures S31–S32).

Scheme 3. Syntheses and Structures of MnN-2, MnN-3, and MnN-4.

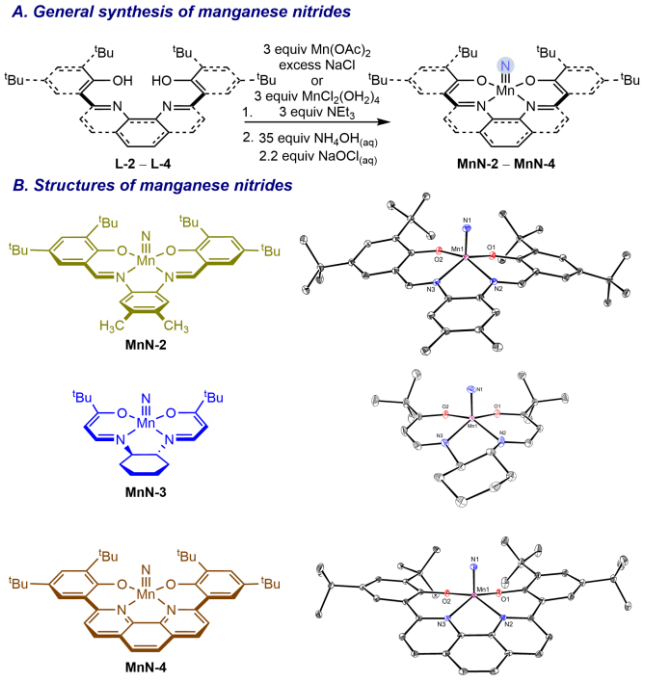

Thermal ellipsoids are shown at 30% probability with hydrogen atoms removed for clarity.

While the IR and crystallographic data suggest little difference between the manganese nitrides, their electronic absorbance spectra are distinct. In THF solution, each compound exhibits a weak absorbance with a local λ_{max} between 600–645 nm with molar extinction coefficients ranging between 160–370 L•mol^{-1}•cm^{-1} (Figure 1). However, the signal with the second lowest energy in the spectra varies greatly with the identity of the supporting ligand with λ_{max} ranging between 326–450 nm with molar extinction coefficients

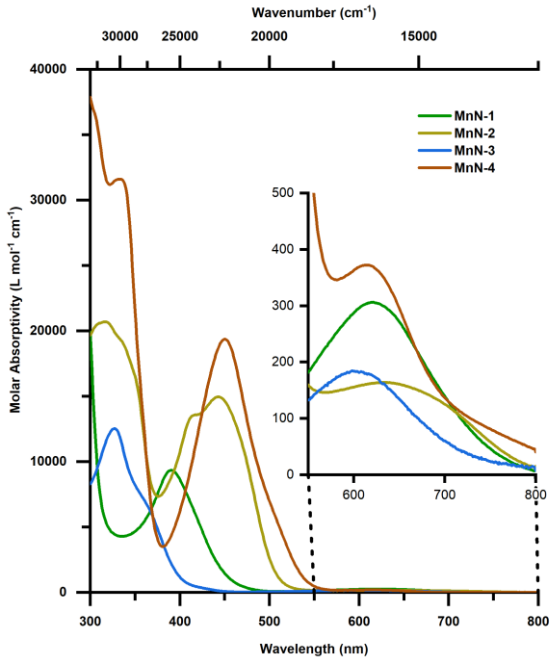

Figure 1. Electronic absorption spectra of manganese nitrides. The electronic absorption spectra in THF of the series of manganese nitrides MnN-1–MnN-4. An inset of the peaks showing the d-d transitions is included.

between 9300–19400 L•mol^{-1}•cm^{-1}. These observations are consistent with previous reports by Gray and coworkers on similar salen-supported manganese(V) nitrides. The lowest energy absorption was assigned as principally a d-d transition, while the higher energy transition was attributed to intraligand charge transfer (ILCT) bands.[15] These assignments are consistent with the observations herein, where the identity of the ligand has very little impact on the energy or intensity of the lower energy band, but the higher energy absorption is dependent on ligand identity. These results further demonstrate that the identity of the N,N,O,O-ligand does not have a major impact on the manganese–nitrogen interaction.

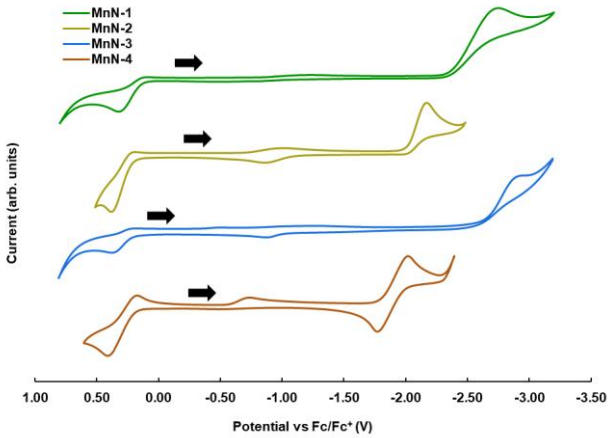

Figure 2. Cyclic voltammograms of manganese nitrides. Solvent: THF; electrolyte: 0.1 M [^{n}Bu$_4$N][PF$_6$]; [analyte] = 0.001 M; ν = 100 mV/s; MnN-1 OCP = −0.35 V vs. Fc/Fc$^+$; MnN-2 OCP = −0.44 V vs. Fc/Fc$^+$; MnN-3 OCP = −0.17 V vs. Fc/Fc$^+$; MnN-4 OCP = −0.17 V vs. Fc/Fc$^+$. Arrow indicates direction of scan and open circuit potential. Signals between –0.25 V vs. Fc/Fc$^+$ and –1.25 V vs. Fc/Fc$^+$ are not observed in the initial scan.

To verify the impact of ligand identity on redox properties of the complex, electrochemical studies were performed. Each experiment was conducted in THF with [NBu$_4$][PF$_6$] as the electrolyte (Figure 2). Analysis of the anodic sweep of the cyclic voltammograms (CV) reveals an irreversible peak between E_{pa}= 0.35 V versus Fc/Fc$^+$ and E_{pa}= 0.41 V versus Fc/Fc$^+$ for all four nitrides. These peaks are consistent with a nitride-centered oxidation, as reported previously.[16] In the cathodic sweep **MnN-1**, **MnN-2**, and **MnN-3** exhibited an irreversible feature at E_{pc}= –2.71, –2.16, and –2.90 V versus Fc/Fc$^+$ respectively assigned as a reduction. **MnN-4** instead showed a reversible reduction wave centered at $E_{1/2}$= –1.88 V versus Fc/Fc$^+$. The breadth of the reduction potential supports a ligand-based redox event. This is consistent with the correlation between reduction potential and increased conjugation (**MnN-3** < **MnN-1** < **MnN-2** < **MnN-4**). Furthermore, while nearby electric fields,[16] electron donating, and electron withdrawing groups[15,17] have been reported to perturb the manganese nitride-based oxidation, the ligands used in this study produced only minor perturbations to this redox event. This observation is consistent with other spectroscopic data that support minimal perturbation of the manganese-nitride but major differences in the ligand-based properties. All nitrides

following either reduction or oxidation show additional peaks between –1.0 and –0.7 V versus Fc/Fc^+ that have been assigned as Mn(II)/Mn(III) redox features from decomposition of the nitride.[15] Initial scans with these peaks absent are reported in Figures S34–S37.

Reactivity of Manganese Nitride Derivatives. Having established that the electronic differences between the manganese nitrides are principally ligand centered, reactivity studies with these compounds were explored. Addition of five equivalents of H_2Acr to a THF solution of each manganese nitride followed by irradiation with 427 nm light under reduced pressure furnished acridine (Acr), ammonia, and a reduced, paramagnetic manganese byproduct. When these studies were conducted in THF, **MnN-4** produced the highest yield of ammonia at 24% yield relative to the manganese nitride (Scheme 4). Using α,α,α-trifluorotoluene ($PhCF_3$) as the solvent significantly increased the yield of ammonia across the series of manganese nitrides. Under these conditions, **MnN-2** proved the most efficient with an 85% yield of free ammonia. **MnN-4** rapidly resulted in a turbid mixture, likely due to the manganese byproduct being insoluble, which is expected to decrease light absorption.

Isotopic labeling studies were conducted to confirm the terminal metal nitride as the N-atom source in the observed NH_3. The synthesis of the ^{15}N isotopologue, **Mn^{15}N-2** was accomplished by using a mixture of $^{15}NH_4Cl$ and NaOH in the place of the NH_4OH solution. The ^1H NMR spectrum of **Mn^{15}N-2** was indistinguishable from the natural abundance isotopologue. Notably a signal was observed at 1054 ppm in the ^{15}N NMR spectrum, diagnostic of a metal nitride (Figure S10). Additionally, the Mn–N stretching frequency of **Mn^{15}N-2** exhibited a redshift to 1023 cm^{-1}, verifying the assignment of the Mn–N stretch (Figure S33). Irradiation of **Mn^{15}N-2** under the standard reaction conditions produced $^{15}NH_3$ exclusively as judged by observation of a doublet rather than a 1:1:1 triplet in the DMSO-d_6 ^1H NMR spectrum (Figure S1). To support H_2Acr as the hydrogen source in ammonia synthesis, 9,10-dihydro-9,10-d_2-acridine-9-d (H_2Acr-d_3) was used and the free ammonia generated from the photodriven reaction was analyzed by trapping as $(ND_{3-x}H_x)BH_3$. The isotopic composition of reaction between ammonia and BH_3 furnished both the ammonia borane adduct $(ND_{3-x}H_x)BH_3$ and cyclotriborazane $[(ND_{2-x}H_x)BH_2]_3$, formed from spontaneous loss of H_xD_{2-x}. Both compounds had deuterium incorporation in the N–H position as judged by ^2H NMR spectroscopy (Figures S2–S3). With the source of the atoms in the produced ammonia confirmed, attention was devoted to understanding the mechanism of formation.

A hypothesis for N–H bond formation with the N,N,O,O-supported manganese nitrides involved photoinitiation. Either an initial electron or effective hydrogen atom transfer event from H_2Acr to the manganese nitride generates a product more thermodynamically poised to participate in PCET (Scheme 5A). Activation of H_2Acr either by electron or H-atom transfer produces an intermediate that contain thermodynamically weaker E-H bonds (dihydroacridine $BDFE_{calc}$= 69 kcal mol^{-1}; dihydroacridinium radical cation $BDFE_{calc}$= 33 kcal mol^{-1}; N-hydroacridine radical $BDFE_{calc}$= 43 kcal mol^{-1}). Upon accepting an H-atom, subsequent additions of H-atom to the manganese intermediates are also more thermodynamically favorable (N–H $BDFE_{calc}$= 60 kcal mol^{-1}; HN–H $BDFE_{calc}$= 84 kcal mol^{-1}; H_2N–H $BDFE_{calc}$= 85 kcal mol^{-1}).[6f]

Scheme 4. Comparison of the reactivity of the manganese nitrides in the H_2Acr photoproduction of ammonia.

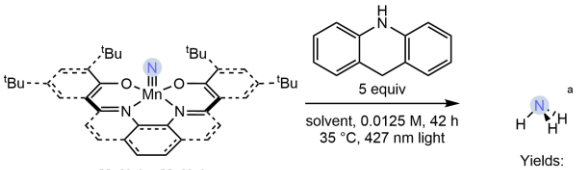

	Yields: THF	$PhCF_3$
MnN-1	3%	40%
MnN-2	10%	85%
MnN-3	12%	40%
MnN-4	24%	28%

MnN 8 mmol; H_2Acr 40 mmol; 5 mL solvent. [a]Ammonia converted into NH_4Cl and measured by ^1H NMR spectroscopy against a CH_2Br_2 internal standard.

While the first PCET event is endergonic, subsequent steps are exergonic. Based on these data, three pathways for the initiation of photodriven ammonia formation were proposed (**Scheme 5**). The first is the photoexcitation of the manganese nitride and PCET or ET occurs with H_2Acr from the excited state. A second possibility is that the manganese nitride and H_2Acr form a donor-acceptor pair in solution and the resulting association complex is responsible for the initial photo-PCET or photo-ET. A final possibility involves H_2Acr as the light absorbing compound and its photoexcited state is responsible for either the initial ET or PCET event.

Scheme 5. Proposed mechanisms for the photoreductions of manganese nitrides by H_2Acr

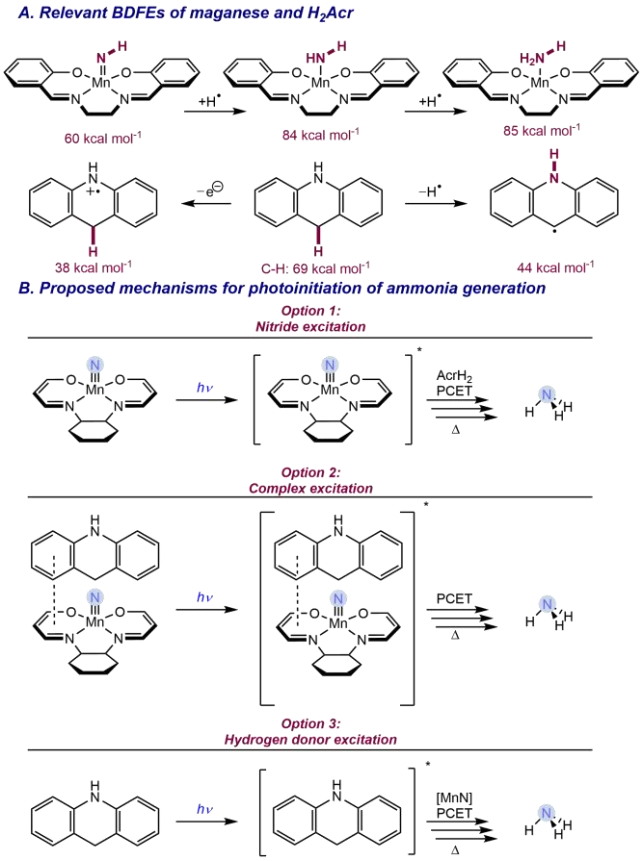

Photophysical Studies of Manganese Nitrides. To evaluate the pathway involving reactivity from the excited state of the

manganese nitride, the excited state lifetimes of each complex was measured using pump-probe transient absorption (TA) spectroscopy. Using a 430 nm pulse to best replicate the conditions of the ammonia synthesis reaction, signals were observed for all four manganese nitride derivatives. However, the signals that were observed did not exceed 100 ps (Figure 3, Figures S53–S68). All of the manganese nitrides studied display bleaching of signals observed in the ground state electronic absorption spectra. In addition, new excited state absorbances (ESAs) were detected at lower energies. These observations are diagnostic of a vibrationally hot ground state, rather than an electronic excited state.[19] No evidence for an observable excited state was obtained, consistent with the excited state lifetime being shorter than the limit of the experiment (< 100 fs). These lifetimes were also invariant in the solvents examined (THF, $PhCF_3$, and 1:1 THF:iPrOH) and inconsistent with the observed experimental solvent effect. Relevant to the ammonia synthesis reaction, such short lifetimes are incompatible with pathways involving a bimolecular reaction between a photoexcited manganese nitride and H_2Acr in solution.

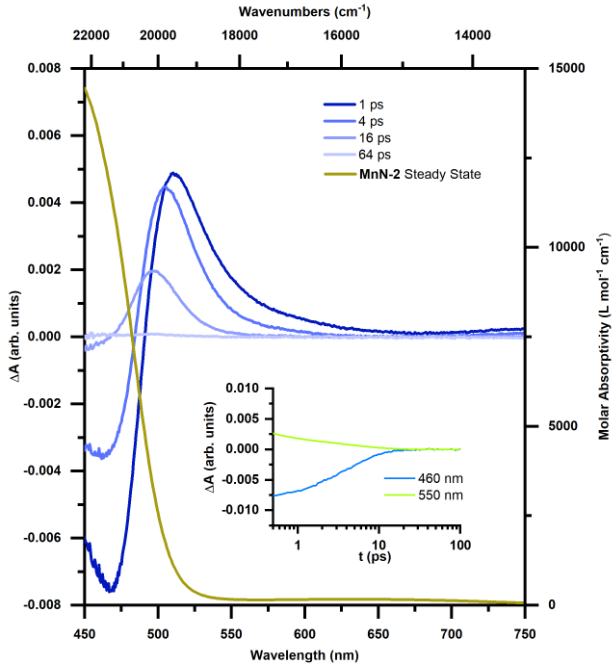

Figure 3. Transient absorption spectra of photoexcited MnN-2 at 23 °C in THF with λ_{exc} = 430 nm and pump power = 600 μW at 1, 4, 16, and 64 ps with a trace of the steady state absorption spectra. Inset contains kinetic data at 460 and 550 nm from 500 fs to 100 ps.

With elimination of a pathway involving an excited-state manganese nitride, the possibility of the interaction of the manganese nitride with H_2Acr in the ground state was explored. Initial experiments focused on the evaluation of the potential of a ground state complex that contains the manganese nitride and H_2Acr in the same shell of solvation. Attempts to obtain evidence of a donor-acceptor complex using electronic absorption spectroscopy revealed minimal changes in the spectrum even at concentrations higher than those of the ammonia synthesis reaction (Figures S46–S49). These observations support no major change in the π-systems of the ligands of the manganese nitrides nor d-orbital splitting in the presence of H_2Acr. Therefore, there is little impact on the two components in solution together in the ground state.

Photophysics of Acridine Derivatives Relevant to Ammonia Formation. With H_2Acr excitation as the remaining option, efforts were then devoted to understanding the excited-state properties of H_2Acr. While photophysical studies on H_2Acr have been reported in the literature previously, these studies focused on the excitation in the ultraviolet region of the electromagnetic spectrum and in relatively dilute solutions.[20] It was important to sublime commercial H_2Acr to obtain material of appropriate purity for photophysical measurements. Impurities present in the commercial samples had little to no impact on catalytic ammonia synthesis, however for all subsequent spectroscopic studies, sublimed material was used exclusively.

Photophysical studies of the purified H_2Acr were initiated using fluorescence spectroscopy. Solutions of H_2Acr in THF irradiated at 310 nm produced a signal at 350 nm with a lifetime of 11 ns. Solutions of H_2Acr in $PhCF_3$ however exhibited no detectable fluorescence, consistent with a new potential non-radiative decay pathway (Figure 4A). Predicting the excited state reduction potential by the sum of the redox event and the excited state energy of H_2Acr in THF produced a value of approximately −3.2 V versus Fc/Fc^+, which is capable of reducing $PhCF_3$ (E_{pc} = −3.1 V versus Fc/Fc^+) to its radical anion.[21] As derivatives of H_2Acr have been targeted for photoreduction,[22] the ability to reduce $PhCF_3$ solvent is plausible. Acr was an observed byproduct of the reaction with manganese nitrides, resulting from oxidation of H_2Acr. In the steps to produce Acr, acridinium ($HAcr^+$) is a potential intermediate. Understanding the interactions between Acr and $HAcr^+$ with H_2Acr is important for understanding the mechanism of the reaction. Examining the fluorescence of Acr and $HAcr^+$ in $PhCF_3$, Acr was irradiated at 370 nm; however no fluorescence was observed in the presence or absence of H_2Acr. $HAcr^+$ was irradiated at 410 nm, which resulted in emission at 482 nm. Lifetime measurements were fit to a triexponential with τ_1, τ_2, and τ_3 being 15.5, 31.1 and 62.1 ns, respectively (Figure 4B). Addition of H_2Acr to $HAcr^+$ resulted in a dramatic quenching of the fluorescence and a drop in the lifetime by an order of magnitude. The decay was fit to a biexponential of τ_1= 1.0 ns and τ_2= 4.0 ns. As H_2Acr is a reductant and $HAcr^+$ is a potential photooxidant, photo-induced electron transfer is a plausible mechanism of interaction between these molecules.

Spectroelectrochemistry was applied to detect intermediates. Electrochemical potentials of H_2Acr were determined in THF using $[NBu_4][PF_6]$ as the supporting electrolyte (Figure 4C). An irreversible oxidation feature at E_{pa} = 0.52 V versus Fc/Fc^+ was observed. By comparison, Acr and $HAcr^+$ displayed a reversible reduction at $E_{1/2}$ = −2.19 V versus Fc/Fc^+ and a quasi-reversible reduction at E_{pc} = −1.01 V versus Fc/Fc^+, respectively (Figure S38). Reduction of Acr at −2.5 V versus Fc/Fc^+ resulted in a series of peaks spanning the visible region consistent with the acridine radical anion (Figure S39).[23] Analyzing the product of reduction of $HAcr^+$ at −1.2 V versus Fc/Fc^+ appeared as a disappearance of the signals associated with $HAcr^+$ (Figure S40) and the precipitation of a white solid at longer times, consistent with the formation of dihydrodiacridine ($(HAcr)_2$) derived from 10-hydroacridine radical ($HAcr^•$). Finally, the oxidation of H_2Acr was evaluated. Oxidation of a solution of H_2Acr in THF resulted in the appearance of a broad peak at 580 nm, signaling formation of a donor-acceptor complex between H_2Acr and $HAcr^+$ (Figure S41). This observation is rationalized by the oxidation of H_2Acr to the 9,10-dihydroacridinium radical cation ($H_2Acr^{+•}$), which, based upon comparison to known alkylated derivatives, is acidic.[6e] $H_2Acr^{+•}$ is capable of protonation of

H_2Acr in solution to produce $HAcr^{\bullet}$ that is further oxidized at the electrode surface to $HAcr^+$. This illustrates the low BDFEs of the N–H and C–H bonds of dihydroacridinium cation are comparable to the N–H and C–H bonds in H_2Acr.

To identify the molecules associated with oxidation and formal H-atom loss from H_2Acr, both pulse radiolysis and TA experiments were employed. Pulse radiolysis (PR) has the ability to generate strong oxidants, reductants, or high energy triplets from the irradiated solvent. As H_2Acr is capable of reducing $PhCF_3$ in its excited state, establishing how the $H_2Acr^{+\bullet}$ radical cation evolves in solution is important for determining its impact in the reaction. While $PhCF_3$ is not a common solvent in PR, the expectation is for it to act similarly to methylene chloride as an oxidant due to its

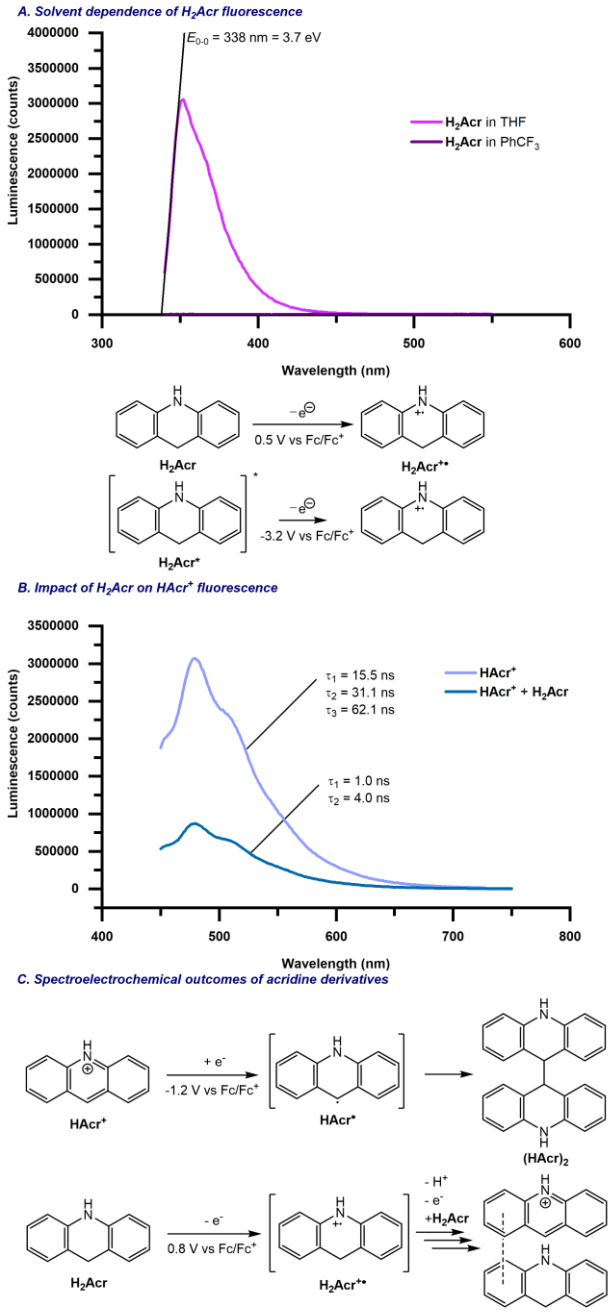

Figure 4. Steady state spectroscopy of acridine derivatives. A. Fluorescence data of H_2Acr in THF and $PhCF_3$. The tangent method along with the measured E_{pa} in THF is used to estimate the excited state oxidation potential, which indicates that the quenching may be from reduction of $PhCF_3$ solvent. B. Excitation spectra of $HAcr^+$ excited at 430 nm in $PhCF_3$. A comparison is made between the presence and absence of saturated solutions of H_2Acr (approximately 25 mM) to quench the excited state with excited state lifetimes included. C. Results of the reduction of $HAcr^+$ and oxidation of H_2Acr. Solvent = THF; electrolyte: 0.1 M [$^nBu_4N$][PF_6].

ability to be reduced and subsequently release halide anion. To support this hypothesis, a solution of 25 mM biphenyl was dissolved in $PhCF_3$ and irradiated with electrons under an atmosphere of either oxygen or argon. At 10 ns after the pulse a positive signal was observed at 370 nm and 660 nm, where the decay of the signal at 680 nm was fit to a biexponential decay with τ_1 and τ_2 are 81.8 ns and 3320 ns, respectively. These signals are characteristic of the biphenyl radical cation (Figure S81).[24] Additionally, some differences between the oxygen and argon purged samples were observed at $\lambda < 400$ nm, which were assigned to biphenyl triplet.[25] However, due to the high quantum efficiency of intersystem crossing of biphenyl, it is difficult to determine if this is from excitation of solvent by pulse radiolysis or Cherenkov radiation.

With demonstration that $PhCF_3$ acts as an oxidant with pulse radiolysis, H_2Acr was then investigated. Under electron irradiation, 25 mM solutions of H_2Acr in $PhCF_3$ produced two states (Figure 5). The first state contains a broad absorbance centered at 660 nm, which is fit to a biexponential decay with τ_1 = 95.6 ns and 1260 ns. The second state exhibits a narrow absorbance centered at 568 nm with a smaller absorbance at 520 nm. The absorbance grew in with a rate of τ = 324 ns and subsequently decayed at $\tau > 14$ µs. The second set of signals survived longer than the experiment window and thus only an estimate of the decay is possible. These results mirror previous results using low temperature radiolysis of H_2Acr in sec-butyl chloride.[23] The first state was identified as $H_2Acr^{+\bullet}$ and the second state as the N-centered radical, 9-hydroacridine radical ($HAcr^{\bullet\prime}$). The second state is likely formed by the deprotonation of dihydroacridinium radical cation by remaining H_2Acr in solution. The expectation that this second signal arises from a bimolecular collision with free H_2Acr in solution is supported by the formation of the second species occurring more slowly at lower concentrations of H_2Acr (1 mM H_2Acr PR in $PhCF_3$, Figure S83). This is an interesting result as $HAcr^{\bullet}$ is the thermodynamically more stable species and$HAcr^{\bullet\prime}$ has been reported to rearrange to $HAcr^{\bullet}$.[23] Both compounds that were detected by PR, $H_2Acr^{+\bullet}$ and $HAcr^{\bullet\prime}$, are expected to have low enough BDFEs to promote donation of an H-atom to the manganese nitrides.[6e] With the lifetime of $HAcr^{\bullet\prime}$ being longer than a microsecond, the likelihood of $HAcr^{\bullet\prime}$ being present to react with manganese nitride is plausible. With signatures of potential H-atom donors derived from oxidation of H_2Acr observed, the ability to generate these species with light was evaluated by TA.

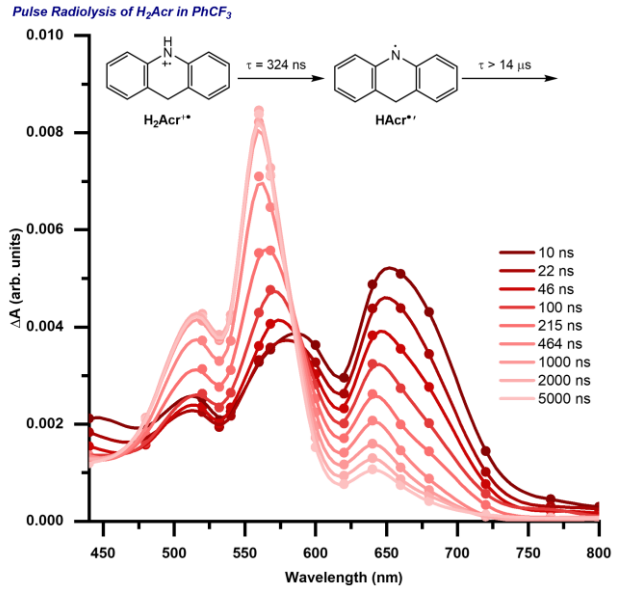

Figure 5. Observation of the H-atom abstracted product from H_2Acr. Pulse radiolysis of 25 mM H_2Acr in $PhCF_3$ saturated with O_2 at 10 ns, 22 ns, 46 ns, 100 ns, 215 ns, 464 ns, 1 µs, 2 µs, and 5 µs.

TA of the isolable acridine derivatives was collected in $PhCF_3$. Samples of H_2Acr in $PhCF_3$ were pumped at 310 nm and resulted in two excited species with ESAs at λ_{max} = 745 nm and λ_{max} = 520 nm, respectively (Figures S72–S74). The first state was fit to a biexponential decay with time constants of τ_1 = 19.1 ps and τ_2 = 395.4 ps. Comparing this to an analogous solution of H_2Acr in THF, two similar states were observed (Figures S69–S71). The first has an ESA at λ_{max} = 758 nm that decays into a second state with an ESA at λ_{max} = 520 nm. The signal at 758 nm was fit to first a biexponential growth with constants equal to τ_1 = 13.6 ps and τ_2 = 1010.2 ps followed by a monoexponential decay fit to τ = 4706.0 ps. These observed signals are likely the same states observed in the $PhCF_3$ sample. While these states are not related to any of the proposed species above, the difference in rate of formation of the second excited state may be of importance, e.g. facilitating the formation of reactive triplet. Upon pumping solutions of Acr in $PhCF_3$ there are two states observed, the first having an ESA at λ_{max} = 557 nm which was fit to a first order decay with a τ = 62 ps (Figures S75–S77). The second state contains ESA at λ_{max} = 444 nm with additional peaks at λ = 484 nm and λ = 518 nm fit to a decay of τ = 22.4 µs and τ = 23.4 µs for the signals at 441 nm and 514 nm, respectively (Figures S78–S80). While only the peak at 444 nm has been reported previously for the triplet state of Acr,[25] the peaks at λ = 484 nm and λ = 518 nm are also likely due to the triplet state of Acr based on the kinetics of the formation of these signals.[21,26] The formation of this species is important, as the triplet state of Acr and its derivatives have been proposed to be responsible for the ability of photoexcited Acr to engage in PCET.[27] Solutions of $HAcr^+$ in $PhCF_3$ pumped at 400 nm or 430 nm resulted in a ground state bleach (GSB) at 440 nm, which persisted longer than the repetition rate of the instrument. This observation is likely due to the high intensity of the fluorescence of the sample. Subtracting this signal from the data revealed ESAs at λ_{max} = 659 nm, λ_{max} = 509 nm and λ_{max} = 464 nm (Figures S81–S85), which were fit to first order decays of 29.7 ns, 26.8 ns and 34.6 ns, respectively.

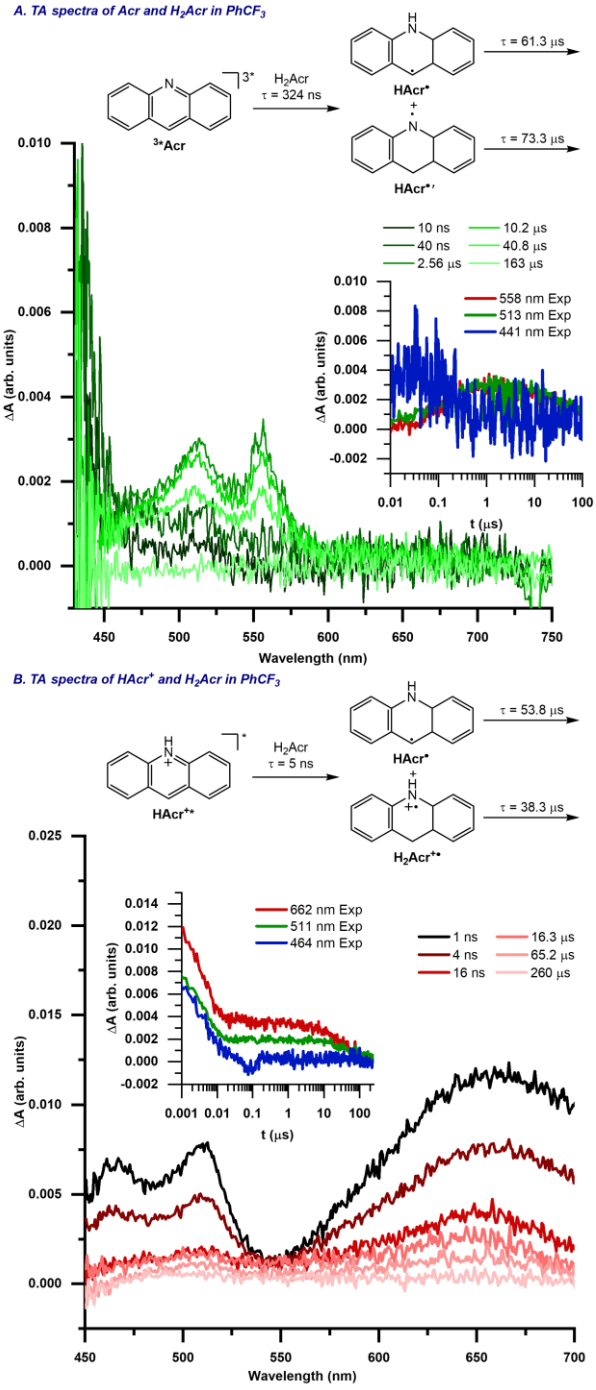

Figure 6. TA spectra of organic byproducts of the reaction and H_2Acr. A. TA spectra of a mixture of Acr and H_2Acr at 23 °C in $PhCF_3$ with λ_{exc} = 370 nm and pump power = 100 µW at 10 ns, 40 ns, 256 µs, 10.2 µs, 40.8 µs and 163 µs. Inset contains kinetic data at 558 nm, 513 nm and 441 nm. Time period ranges from 10 ns to 100 µs. B. TA spectra of a mixture of $HAcr^+$ and H_2Acr at 23 °C in $PhCF_3$ with λ_{exc} = 400 nm and pump power = 150 µW at 1 ns, 4 ns, 16 ns, 16.3 µs, 65.2 µs, and 260 µs. Inset contains kinetic data at 662 nm, 511 nm and 464 nm. Time period ranges from 1 ns to 250 µs.

As Acr and H_2Acr are known to react in the solid state to produce $HAcr^•$ and $HAcr^{•'}$,[28] a solution of Acr and H_2Acr in $PhCF_3$ was pumped at 370 nm. While at short times the peaks at 441 nm, 484 nm and 514 nm were observed, their lifetimes were shorter than solutions containing simply Acr. Furthermore,

additional signals were observed at long times centered at λ = 513 nm and λ = 558 nm. The signal at 441 nm decayed at a rate of τ = 230 ns, and the growth of the new signals was fixed to a growth rate of τ = 200 ns and subsequent decays at τ = 61.3 μs and τ = 73.3 μs for the signals at 513 nm and 558 nm respectively (Figure 6A). The signal at 513 nm was identified as $HAcr^{\bullet}$ and the signal at 558 nm was identified as $HAcr^{\bullet\prime}$.[23] These species arise from an intermolecular PCET event between triplet Acr and H_2Acr, followed by the reverse reaction to ground state Acr and H_2Acr. These results agree with previously reported EPR studies in the solid state and show this process occurs in solution.[28] Solutions of $HAcr^+$ and H_2Acr in $PhCF_3$ resulted in a short and long decay components at 511 nm and 662 nm fit to τ_1 = 5 ns, τ_2 = 53.8 μs and τ_1 = 5 ns, τ_2 = 38.3 μs (Figure 6B). These long-lived signals were identified as $HAcr^{\bullet}$ and $H2Acr^{+\bullet}$, that arise from intermolecular single electron transfer (SET) from excited state $HAcr^+$ and H_2Acr. These species then undergo SET to regenerate $HAcr^+$ and H_2Acr. Rapid production of insoluble $(HAcr)_2$ at the point of irradiation was observed in both experiments, which is generated from $HAcr^{\bullet}$ present in solution.

Proposed Mechanism and Improved Photoreactivity of Manganese Nitrides. A mechanism of precious metal-free photodriven ammonia synthesis based on the spectroscopic data is presented in Scheme 6. A small amount of H_2Acr is photoexcited to generate a highly reducing excited state. This excited state either reduces the manganese nitride or solvent in the case of $PhCF_3$, as supported by fluorescence quenching, to generate $H_2Acr^{+\bullet}$. **MnN-2** and **MnN-4** are the optimal substrates as they are the most readily reduced. Because $H_2Acr^{+\bullet}$ is acidic and has low BDFEs,[6g] it readily engages in PCET with the manganese nitride to generate a reactive manganese imido and $HAcr^+$. The $HAcr^+$ serves as a photooxidant, engaging in SET with H_2Acr to generate $HAcr^{\bullet}$ and $H_2Acr^{+\bullet}$, as supported by fluorescence quenching and TA measurements. Both the produced $HAcr^{\bullet}$ and $H_2Acr^{+\bullet}$ are capable of reacting with manganese nitride to generate the manganese parent imido and Acr or $HAcr^+$ respectively. The manganese imido undergoes additional reactions with H_2Acr to generate ammonia, Acr, and manganese(II) products. As H_2Acr is a poor absorber of visible light, additional radical chains are generated by excited state Acr that engages in PCET with H_2Acr generating reactive $HAcr^{\bullet}$. This PCET is a known reaction from the T_1 state of Acr and was observed in TA experiments.[28] The resulting two equivalents of $HAcr^{\bullet}$ engage in PCET with two equivalents of manganese nitride to produce manganese imido. This produces more ammonia, manganese products, and importantly Acr that engages with H_2Acr again.

Scheme 6. Proposed mechanism of photoinitiated ammonia synthesis from manganese nitrides and H_2Acr

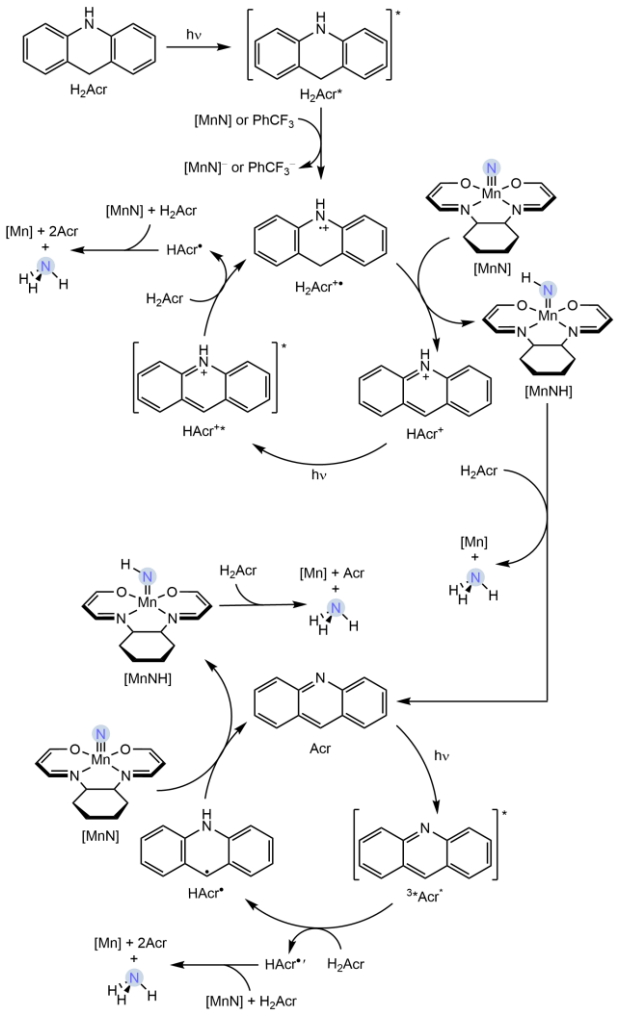

Based on the proposed mechanism addition of Acr at the beginning of the reaction, was hypothesized to greatly increase the rate of reaction. The reaction of **MnN-2** and H_2Acr at 16 h resulted in a 44% yield with 26% remaining nitride. Addition of 10 mol% of acridine to the reaction resulted in a 69% yield with 12% remaining nitride. This increase in relative rate is consistent with the formation of intermediates proposed based on the spectroscopic data.

Scheme 7. Impact of Acr on the formation of ammonia.

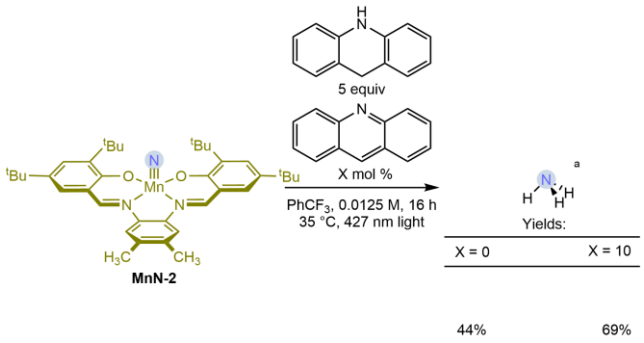

[a]NH_3 production determined by ^1H NMR integration as NH_4Cl vs. CH_2Br_2 internal standard.

CONCLUSION

By tuning the ligand supporting a manganese(V) nitride, ammonia synthesis superior to that observed with precious metal

photocatalysts has been observed. The mechanistic investigation led by TA spectroscopy established that this ligand effect had little impact on the photophysics of the metal nitride but instead was correlated with the ability of the compound to accept electrons. Accepting electrons either by the ligand or the solvent is pivotal towards the activation of the source of the proton and the electron, H_2Acr. Oxidation of H_2Acr results in the production of $H_2Acr^{+\bullet}$, $HAcr^{\bullet}$ and $HAcr^{\bullet\prime}$, which were all observed by TA experiments and all contain weak E–H bonds. This work is expected to have implications for future work into photodriven ammonia synthesis.

ASSOCIATED CONTENT

Supporting Information

The Supporting Information is available free of charge on the ACS Publications website.

AUTHOR INFORMATION

Corresponding Authors

Paul J. Chirik — Department of Chemistry, Princeton University, Princeton, New Jersey 08544, United States; orcid.org/0000-0001-8473-2898; Email: pchirik@princeton.edu

Gregory D. Scholes — Department of Chemistry, Princeton University, Princeton, New Jersey 08544, United States; orcid.org/0000-0003-3336-7960; Email: gscholes@princeton.edu

Matthew J. Bird - Chemistry Division, Brookhaven National Laboratory, Upton, New York 11973, United States; https://orcid.org/0000-0002-6819-5380; Email: mbird@bnl.gov

Authors

Grace B. Panetti — Department of Chemistry, Princeton University, Princeton, New Jersey 08544, United States; orcid.org/0000-0001-7833-5706

Junho Kim — Department of Chemistry, Princeton University, Princeton, New Jersey 08544, United States; orcid.org/0000-0002-8977-2925

Michele S. Myong - Chemistry Division, Brookhaven National Laboratory, Upton, New York 11973, United States; orcid.org/0000-0003-3634-8933

Author Contributions

The manuscript was written through contributions of all authors. All authors have given approval to the final version of the manuscript.

Funding Sources

Any funds used to support the research of the manuscript should be placed here (per journal style).

Notes

Any additional relevant notes should be placed here.

ACKNOWLEDGMENT

This research was supported by BioLEC, an Energy Frontier Research Center funded by the U.S. Department of Energy, Office of Science, Basic Energy Sciences, under Award DE-SC0019370 (transient absorption, pulse radiolysis, and luminescence studies). P.J.C. and G.B.P. were also supported by the U.S. Department of Energy, Office of Science, Office of Basic Energy Sciences, Catalysis Science program, under Award DE-SC0006498 (manganese nitride syntheses and reactivity studies). Use of the Laser Electron Accel-erator Facility (LEAF) of the BNL Accelerator Center for Energy Research (ACER) was supported by U.S. Department of Energy, Office of Science, Office of Basic Energy Sciences, Division of Chemical Sciences, Geosciences & Bioscience through contract DE-SC0012704. We also thank Prof. Felix Castellano and group for helpful discussions.

REFERENCES

(1) (a) Luo, Q.; Lu, C.; Liu, L.; Zhu, M. A review on the synthesis of transition metal nitride nanostructures and their energy related applications. *GEE* **2023,** *8* , 406-437. (b) Wang, H.; Li, J.; Li, K.; Lin, Y.; Chen, J.; Gao, L.; Nicolosi, V.; Xiao, X.; Lee, J.-M. Transition metal nitrides for electrochemical energy applications. *Chem. Soc. Rev.* **2021,** *50*, 1354-1390. (c) Cheng, Z.; Qi, W.; Pang, C. H.; Thomas, T.; Wu, T.; Liu, S.; Yang, M. Recent Advances in Transition Metal Nitride-Based Materials for Photocatalytic Applications. *Adv. Funct. Mater.* **2021,** *31*, 2100553. (d) Eikey, R. A.; Abu-Omar, M. M. Nitrido and imido transition metal complexes of Groups 6–8. *Coord. Chem. Rev.* **2003,** *243*, 83-124. (e) Berry, J. F. Terminal Nitrido and Imido Complexes of the Late Transition Metals. *Comments on Inorganic Chemistry* **2009,** *30*, 28-66.

(2) (a) Du Bois, J.; Tomooka, C. S.; Hong, J.; Carreira, E. M. Nitridomanganese(V) Complexes: Design, Preparation, and Use as Nitrogen Atom-Transfer Reagents. *Acc. Chem. Res.* **1997,** *30*, 364-372. (b) Smith, J. M. Reactive Transition Metal Nitride Complexes. In *Progress in Inorganic Chemistry Volume 58*, 2014; pp 417-470. (c) Kelly, P. Q.; Filatov, A. S.; Levin, M. D. A Synthetic Cycle for Heteroarene Synthesis by Nitride Insertion. *Angew. Chem. Int. Ed.* **2022,** *61*, e202213041.

(3) (a) Kim, S.; Park, Y.; Kim, J.; Pabst, T. P. Chirik, P. J., Ammonia synthesis by photocatalytic hydrogenation of a N_2-derived molybdenum nitride. *Nature Synthesis* **2022,** *1*, 297-303. (b) Bruch, Q. J.; Connor, G. P.; Chen, C.-H.; Holland, P. L.; Mayer, J. M.; Hasanayn, F.; Miller, A. J. M. Dinitrogen Reduction to Ammonium at Rhenium Utilizing Light and Proton-Coupled Electron Transfer. *J. Am. Chem. Soc.* **2019,** *141*, 20198-20208. (c) Bezdek, M. J.; Pappas, I.; Chirik, P. J. Determining and Understanding N-H Bond Strengths in Synthetic Nitrogen Fixation Cycles. In *Nitrogen Fixation*, Nishibayashi, Y., Ed. Springer International Publishing: Cham, 2017; pp 1-21. (d) Ashida, Y.; Mizushima, T.; Arashiba, K.; Egi, A.; Tanaka, H.; Yoshizawa, K.; Nishibayashi, Y. Catalytic production of ammonia from dinitrogen employing molybdenum complexes bearing N-heterocyclic carbene-based PCP-type pincer ligands. *Nat. Catal.* **2023**, *2*, 635-644.

(4) (a) Ashida, Y.; Egi, A.; Arashiba, K.; Tanaka, H.; Mitsumoto, T.; Kuriyama, S.; Yoshizawa, K.; Nishibayashi, Y. Catalytic Reduction of Dinitrogen into Ammonia and Hydrazine by Using Chromium Complexes Bearing PCP-Type Pincer Ligands. *Chem. -Eur. J.* **2022,** *28*, e202200557. (b) Eizawa, A.; Arashiba, K.; Tanaka, H.; Kuriyama, S.; Matsuo, Y.; Nakajima, K.; Yoshizawa, K.; Nishibayashi, Y. Remarkable catalytic activity of dinitrogen-bridged dimolybdenum complexes bearing NHC-based PCP-pincer ligands toward nitrogen fixation. *Nat. Commun.* **2017,** *8*, 14874. (c) Chalkley, M. J.; Drover, M. W.; Peters, J. C., Catalytic N_2-to-NH_3 (or -N_2H_4) Conversion by Well-Defined Molecular Coordination Complexes. *Chem. Rev.* **2020,** *120*, 5582-5636.

(5) (a) Gentry, E. C.; Knowles, R. R. Synthetic Applications of Proton-Coupled Electron Transfer. *Acc. Chem. Res.* **2016,** *49*, 1546-1556. (b) Park, Y.; Kim, S.; Tian, L.; Zhong, H.; Scholes, G. D.; Chirik, P. J. Visible light enables catalytic formation of weak chemical bonds with molecular hydrogen. *Nat. Chem.* **2021,** *13*, 969-976.

(6) (a) Chciuk, T. V.; Anderson, W. R., Jr.; Flowers, R. A., II, Proton-Coupled Electron Transfer in the Reduction of Carbonyls by Samarium Diiodide–Water Complexes. *J. Am. Chem. Soc.* **2016,** *138*, 8738-8741. (b) Chciuk, T. V.; Li, A. M.; Vazquez-Lopez, A.; Anderson, W. R., Jr.; Flowers, R. A., II, Secondary Amides as Hydrogen Atom Transfer Promoters for Reactions of Samarium Diiodide. *Org. Lett.* **2017,** *19*, 290-293. (c) Bezdek, M. J.; Guo, S.; Chirik, P. J.

Coordination-induced weakening of ammonia, water, and hydrazine X–H bonds in a molybdenum complex. *Science* **2016,** *354*, 730-733. (d) Bezdek, M. J.; Pelczer, I.; Chirik, P. J. Coordination-Induced N–H Bond Weakening in a Molybdenum Pyrrolidine Complex: Isotopic Labeling Provides Insight into the Pathway for H_2 Evolution. *Organometallics* **2020,** *39*, 3050-3059. Stratakes, B. M.; Wells, K. A.; Kurtz, D. A.; Castellano, F. N.; Miller, A. J. M. Photochemical H_2 Evolution from Bis(diphosphine)nickel Hydrides Enables Low-Overpotential Electrocatalysis. *J. Am. Chem. Soc.* **2021**. *143*. 21388-21401. (f) Warren, J. J.; Tronic, T. A.; Mayer, J. M. Thermochemistry of Proton-Coupled Electron Transfer Reagents and its Implications. *Chem. Rev.* **2010,** *110*, 6961-7001. (g) Wang, D.; Loose, F.; Chirik, P. J.; Knowles, R. R., N–H Bond Formation in a Manganese(V) Nitride Yields Ammonia by Light-Driven Proton-Coupled Electron Transfer. *J. Am. Chem. Soc.* **2019,** *141*, 4795-4799.

(7) Murray, P. R. D.; Cox, J. H.; Chiappini, N. D.; Roos, C. B.; McLoughlin, E. A.; Hejna, B. G.; Nguyen, S. T.; Ripberger, H. H.; Ganley, J. M.; Tsui, E.; Shin, N. Y.; Koronkiewicz, B.; Qiu, G.; Knowles, R. R., Photochemical and Electrochemical Applications of Proton-Coupled Electron Transfer in Organic Synthesis. *Chem. Rev.* **2022,** *122*, 2017-2291.

(8) Loose, F.; Wang, D.; Tian, L.; Scholes, G. D.; Knowles, R. R.; Chirik, P. J., Evaluation of excited state bond weakening for ammonia synthesis from a manganese nitride: stepwise proton coupled electron transfer is preferred over hydrogen atom transfer. *Chem. Commun.* **2019,** *55*, 5595-5598.

(9) Ashida, Y.; Onozuka, Y.; Arashiba, K.; Konomi, A.; Tanaka, H.; Kuriyama, S.; Yamazaki, Y.; Yoshizawa, K.; Nishibayashi, Y. Catalytic nitrogen fixation using visible light energy. *Nat. Commun.* **2022,** *13*, 7263.

(10) Johansen, C. M.; Boyd, E. A.; Peters, J. C. Catalytic transfer hydrogenation of N_2 to NH_3 via a photoredox catalysis strategy. *Science Advances* **2022,** *8*, eade3510.

(11) (a) Borovik, A. S. Role of metal–oxo complexes in the cleavage of C–H bonds. *Chem. Soc. Rev.* **2011,** *40*, 1870-1874. (b) Harischandra, D. N.; Zhang, R.; Newcomb, M. Photochemical Generation of a Highly Reactive Iron−Oxo Intermediate. A True Iron(V)−Oxo Species? *J. Am. Chem. Soc.* **2005,** *127*, 13776-13777. (c) Capaldo, L.; Ravelli, D.; Fagnoni, M. Direct Photocatalyzed Hydrogen Atom Transfer (HAT) for Aliphatic C–H Bonds Elaboration. *Chem. Rev.* **2022,** *122*, 1875-1924. (d) Cowie, B. E.; Purkis, J. M.; Austin, J.; Love, J. B.; Arnold, P. L. Thermal and Photochemical Reduction and Functionalization Chemistry of the Uranyl Dication, $[U^{VI}O_2]^{2+}$. *Chem. Rev.* **2019,** *119*, 10595-10637.

(12) (a) Xue, W.-M.; Wang, Y.; Mak, T. C. W.; Che, C.-M. Photoluminescence, photoredox properties and crystal structures of rhenium(V)–benzylidyne complexes with phosphine ligands. *J. Chem. Soc. Dalton Trans.* **1996**, 2827-2834. (b) Lovaasen, B. M.; Lockard, J. V.; Cohen, B. W.; Yang, S.; Zhang, X.; Simpson, C. K.; Chen, L. X.; Hopkins, M. D. Ground-State and Excited-State Structures of Tungsten–Benzylidyne Complexes. *Inorg. Chem.* **2012,** *51*, 5660-5670.

(13(a) Chin, K.-F.; Cheung, K.-K.; Yip, H.-K.; Mak, T. C. W.; Che, C. M. Luminescent nitridometal complexes. Photophysical and photochemical properties of the 3[(d)1(dπ*)1] excited state of nitridoosmium(VI) complexes with polypyridine ligands. *J. Chem. Soc. Dalton Trans.* **1995**, 657-663. (b) Lai, S.-W.; Lau, T.-C.; Fung, W. K. M.; Zhu, N.; Che, C.-M. Luminescent Nitridoosmium(VI) Complexes with Aryl- and Alkylacetylide Ligands: Spectroscopic Properties and Crystal Structures. *Organometallics* **2003,** *22*, 315-320. (c) Ikeda, H.; Ito, A.; Sakuda, E.; Kitamura, N.; Takayama, T.; Sekine, T.; Shinohara, A.; Yoshimura, T., Excited-State Characteristics of Tetracyanidonitridorhenium(V) and -technetium(V) Complexes with N-Heteroaromatic Ligands. *Inorg. Chem.* **2013,** *52*, 6319-6327. (d) Wing-Wah Yam, V.; Pui, Y.-L.; Man-Chung Wong, K.; Cheung, K.-K. Synthesis, structural characterisation, photophysics, photochemistry and electrochemistry of nitrido- and trans-dioxorhenium(V) complexes with substituted dppe ligands (dppe=bis(diphenylphosphino)ethane). *Inorg. Chim. Acta* **2000,** *300-302*, 721-732. (e) Bailey, S. E.; Eikey, R. A.; Abu-Omar, M. M.; Zink, J. I. Excited-State Distortions Determined from Structured Luminescence of Nitridorhenium(V) Complexes. *Inorg. Chem.* **2002,** *41*, 1755-1760.

(14) Svenstrup, N.; Bøgevig, A.; G. Hazell, R.; Anker Jørgensen, K. Enantioselective α-amination of ketones mediated by chiral nitridomanganese(V) complexes using ammonia as the terminal nitrogen source. *J. Chem. Soc. Perkin Trans. 1* **1999**, 1559-1566.

(15) Chang, C. J.; Connick, W. B.; Low, D. W.; Day, M. W.; Gray, H. B. Electronic Structures of Nitridomanganese(V) Complexes. *Inorg. Chem.* **1998,** *37*, 3107-3110.

(16) Clarke, R. M.; Storr, T. Tuning Electronic Structure To Control Manganese Nitride Activation. *J. Am. Chem. Soc.* **2016,** *138*, 15299-15302.

(17) Léonard, N. G.; Chantarojsiri, T.; Ziller, J. W.; Yang, J. Y. Cationic Effects on the Net Hydrogen Atom Bond Dissociation Free Energy of High-Valent Manganese Imido Complexes. *J. Am. Chem. Soc.* **2022,** *144*, 1503-1508.

(18) Hein, N. M.; MacNeil, G. A.; Storr, T. Elaboration on the Electronics of Salen Manganese Nitrides: Investigations into Alkoxy-Substituted Ligand Scaffolds. *Inorg. Chem.* **2021,** *60*, 16895-16905.

(19) Schluschaß, B.; Borter, J.-H.; Rupp, S.; Demeshko, S.; Herwig, C.; Limberg, C.; Maciulis, N. A.; Schneider, J.; Würtele, C.; Krewald, V.; Schwarzer, D.; Schneider, S. Cyanate Formation via Photolytic Splitting of Dinitrogen. *JACS Au* **2021,** *1*, 879-894.

(20) Adams, J. E.; Mantulin, W. W.; Huber, J. R. Effect of molecular geometry on spin-orbit coupling of aromatic amines in solution. Diphenylamine, iminobibenzyl, acridan, and carbazole. *J. Am. Chem. Soc.* **1973,** *95*, 5477-5481.

(21) Clavel, P.; Lessene, G.; Biran, C.; Bordeau, M.; Roques, N.; Trévin, S.; Montauzon, D. d. Selective electrochemical synthesis and reactivity of functional benzylic fluorosilylsynthons. *J. Fluor. Chem.* **2001,** *107*, 301-310.

(22) Buss, B. L.; Lim, C.-H.; Miyake, G. M. Dimethyl Dihydroacridines as Photocatalysts in Organocatalyzed Atom Transfer Radical Polymerization of Acrylate Monomers. *Angew. Chem. Int. Ed.* **2020,** *59*, 3209-3217.

(23) (a) Kira, A.; Koizumi, M. Photochemistry of Acridine and Acridan. Two Isomeric forms of Acridine Semiquinone. *Bull. Chem. Soc. Jpn.* **1969,** *42*, 625-630. (b) Shida, T.; Kira, A. Spectroscopic Studies on Radicals Produced from Acridine and Acridan in γ-Irradiated Rigid Solutions at −196°C. *Bull. Chem. Soc. Jpn.* **1969,** *42*, 1197-1201.

(24) Sehested, K.; Hart, E. J. Formation and Decay of the Biphenyl Cation Radical in Aqueous Acidic Solution. *J. Phys. Chem.* **1975,** *79* , 1639-1642.

(25) Naik, D.B.; Dey, G. R.; Kishore, K.; Moorthy, P. N. Studies of the triplet state of biphenyl derivatives by nanosecond pulse radiolysis. *J. Photochem. Photobiol., A* **1992**, *68*, 337-342.

(26) (a) Tokumura, K.; Kikuchi, K.; Koizumi, M. Determination of the Intersystem Crossing Probabilities of Acridine in Various Alcohols. *Bull. Chem. Soc. Jpn.* **1973,** *46*, 1309-1315. (b) Kikuchi, K.; Uji-ie, K.; Miyashita, Y.; Kokubun, H. Intersystem Crossing Processes of Acridine. *Bull. Chem. Soc. Jpn.* **1977,** *50*, 879-882.

(27) (a) Miyashita, Y.; Niizuma, S.; Kokubun, H.; Koizumi, M. Reactive States of Acridine for the Photoreduction in Tetrahydrofuran. *Bull. Chem. Soc. Jpn.* **1970,** *43*, 3435-3443. (b) Hoshino, M.; Koizumi, M. Photochemistry of Acridines. XIX. Photoreduction of Acridine in Mixed Solvents. *Bull. Chem. Soc. Jpn.* **1973,** *46*, 745-748. (c) Eisenhart, T. T.; Dempsey, J. L. Photo-induced Proton-Coupled Electron Transfer Reactions of Acridine Orange: Comprehensive Spectral and Kinetics Analysis. *J. Am. Chem. Soc.* **2014,** *136*, 12221-12224.

(28) Niizuma, S.; Kokubun, H.; Koizumi, M. Four Radical Species Produced Photochemically in the Solid Mixture of Acridine and Acridan. *Bull. Chem. Soc. Jpn.* **1971,** *44*, 335-341.

For Table of Contents Use